Please do not adjust margins

Journal Name

ARTICLE

A microfluidic device for characterizing nuclear deformations

Received 00th January 20xx,
Accepted 00th January 20xx

DOI: 10.1039/x0xx00000x

www.rsc.org/

Andrew C. Hodgson[*,1], Christophe M. Verstreken[*,1,2], Cynthia L. Fisher, Ulrich F. Keyser[1], Stefano Pagliara[^,3] and Kevin J. Chalut[^,1,2]

Cell nuclei experience and respond to a wide range of forces, both *in vivo* and *in vitro*. In order to characterize the nuclear response to physical stress, we developed a microfluidic chip and used it to apply mechanical stress to live cells and measure their nuclear deformability. The device design is optimized for the detection of both nucleus and cytoplasm, which can then be conveniently quantified using a custom-written Matlab program. We demonstrated quantitative measurements of the nuclear sizes and strains of embryonic stem cells, for which we observed negative Poisson ratios in the nuclei for specific medium conditions. In addition, we were able to detect changes in the nuclear response after treatment with actin depolymerizing and chromatin decondensing agents. Finally, we showed that the device can be used for biologically relevant high-resolution confocal imaging of cells under compression. Thus, the device presented here allows for accurate physical phenotyping at high throughput and has the potential to be applied to a range of cell types.

Introduction

Cells experience a wide range of chemical and physical cues from their microenvironment, but the biological and physical relevance of these signals are not well understood. On the one hand, the external physical environment has been shown to affect cell fate and development, for example by influencing lineage commitment of ES cells upon differentiation.[1,2] On the other hand, the phenotype of the cell, such as cell type and differentiation state, can drive changes in cell mechanics. For example, large changes in nuclear organization and stiffness during key developmental stages have been observed.[3,4] Given the precision with which the physical and chemical environment can be controlled, and the capability for high throughput measurements, microfluidic devices are an ideal platform to explore the effects of external stresses on the biological and biophysical processes occurring in single cells.[5]

The prevalence and sophistication of microfluidic devices in the study of cellular biophysics has increased in recent years.[6,7] A wide range of assays now exist to modify the environment of a variety of cells, including controlling chemical gradients,[8] rapid cell sorting[9] and high throughput phenotyping.[10,11] The scale of microfluidic devices allows for parallelized measurements at the single-cell level, while simultaneously greatly reducing reagent usage compared to traditional techniques.[12] For example, microfluidic devices have recently been used to uncover the physical behavior of embryonic stem (ES) cells in response to external signals, providing physiologically relevant information for *in vitro* investigations.[13]

In this paper we introduce a microfluidic platform for the high-throughput measurement of cellular and nuclear deformability of ES cells whose mechanics have been shown to alter as the cells exit pluripotency and initiate lineage choice.[14] The device consists of a chip made of polydimethylsiloxane (PDMS), prepared in advance of the experiment day and finalized using a 30-minute procedure. This permits short setup times and straightforward use by a cell biologist with little or no experience with microfluidics, while assuring repeatability in terms of the physical and chemical environment inside the chip as to minimize the impact on cell viability and culture quality.

Before the experiment, cells are labelled with SYTO 13 (Invitrogen), a fluorescent nucleic acid marker to illuminate the nucleus with an intensity that is 3-4 times higher than the

* *These authors contributed equally*
[1] *Cavendish Laboratory, Department of Physics, University of Cambridge, Cambridge CB3 0HE, UK*
[2] *Wellcome Trust/Medical Research Council Cambridge Stem Cell Institute and Department of Clinical Neurosciences, University of Cambridge, Cambridge CB3 0ES, UK*
[3] *Department of Biosciences, College of Life and Environmental Sciences, University of Exeter, Exeter, Devon EX4, United Kingdom*
^ *Corresponding authors: s.pagliara@exeter.ac.uk, kc370@cam.ac.uk*
Electronic Supplementary Information (ESI) available: [details of any supplementary information available should be included here]. See DOI: 10.1039/x0xx00000x

This journal is © The Royal Society of Chemistry 20xx

Please do not adjust margins

Please do not adjust margins

cytoplasm.[15] This allows easy visualization and detection of the nucleus and the surrounding cytoplasm inside the chip. The cells, when loaded into the chip, are flowed in suspension and a compression force is applied by confining them in a channel slightly smaller than their cross-sectional area. The cells are imaged before, during and after compression. A custom Matlab GUI analyzes such images and calculates cellular and nuclear strain, or deformability, allowing for assessing the cellular and nuclear response to physical stress. Deformability is a proxy for cell and nuclear mechanics, which correlates with cell states in development and disease.[16-18] In this manner, the device can be used for accurate mechanical phenotyping and identifying various stages of development while simultaneously providing valuable data on the physical biology of cells at those stages.

Experimental

Design and production of the molds

The mask was designed using AutoCAD (Autodesk). The designs were translated into a photomask (Photodata) and printed onto an emulsion film with a resolution of 128,000 dpi to be used for photolithography. The 16 µm structures, serving as a template to produce reservoirs and compression channels in the subsequent step (see below) were deposited onto a silicon wafer using a single lithography step as follows. SU-8 2015 (Microchem) was spin-coated onto the wafer at 3000 rpm for 60 s after a ramp of 300 rpm per second. A UV lamp (365-405 nm, 20 mW cm^{-2}) was used to expose the mask onto the deposited photoresist for 6s. After post-baking for 5 min and developing in propylene glycol monomethyl ether acetate (PGMEA) (Sigma-Aldrich), the wafer contained SU-8 structures with a height of 16 µm as verified using a stylus profilometer (Dektak). The dimensions of this device are reported in Fig. 1.

Production of microfluidic chip & experimental procedure

A device negative replica was produced by placing the silicon wafer into an open container with base surface area slightly larger than the wafer itself. The wafer was then covered with degassed 9:1 (base : curing agent) polydimethylsiloxane (PDMS) and cured at 70 °C for 60 min, before the area around the features was cut with a scalpel to remove the microfluidic chip from the mold. A 1.5 mm biopsy punch (Kai Medical) was used to create fluidic accesses to the chip at the outer ends of both reservoirs. Oxygen plasma treatment (10s exposure at 100 W, Diener) was used to bond the patterned surface of the PDMS chip to a glass slide (24x50 mm, 0.13-0.16 mm, Menzel-Gläser). This treatment temporarily renders PDMS and glass hydrophilic, so within 5 min after bonding the chips were filled with the cell culture medium that would be used during imaging. FEP tubing (1/16 in×0.03 in, outer and inner diameters respectively, Gilson) was used to connect the reservoirs to a pressurized microfluidic flow control system (MFCS-4C, Fluigent). The inlet tube was filled with a cell suspension while the outlet tube was filled with cell culture media pre-equilibrated to culture conditions by incubating it at 37 °C and 7% CO_2. The flow across the constriction channels was controlled using the MFCS-4C's computer software (MAESFLO, Fluigent). Imaging was performed on a Leica SP5 in epifluorescence mode, using a 20x/0.5N.A. objective and 2x2 binning. For translocation measurements, the microfluidic chip was connected to a syringe pump (Nemesys, Cetoni) to supply a constant flow of 100 µl/min for each of the samples. Translocation measurements were performed by only imaging the region of interest and using 4x4 binning on an Olympus IX73 epifluorescence microscope using a 20x/0.5N.A. Olympus objective and an optiMos sCMOS camera. 3D imaging on Lifeact-tagRFP cells was performed using a 40x/1.30N.A. objective on a Nikon Eclipse Ti spinning disk confocal microscope. 3D images were reconstructed using Volocity (PerkinElmer). For each data set, a new microfluidic chip casted out of the same mold was used. The measurement error was estimated using (9.9±0.12) µm green-yellow fluorescently labelled beads (10µm Fluorospheres, Thermo Fisher).

Preparation of cells for microfluidic analysis

This study used wild type ES cells derived from 129/Sv strain mice, and cells of the same type but transfected with a Lifeact-tagRFP plasmid (ibidi). We received the ES cell as a kind gift from Jennifer Nichols's laboratory at the University of Cambridge. The cells were cultured at 37 °C and 7% CO_2 in medium based on Glasgow Eagle's Minimal Essential Medium (Merck), supplemented with 10% HyClone Fetal Bovine Serum (GE), L-glutamine (Invitrogen), MEM Non-Essential Amino Acids (PAA), Sodium Pyruvate (Invitrogen), ß-mercaptoethanol (Sigma) and LIF (Millipore).[19] For routine culture, cells were incubated at 37 °C in 7% CO_2 and split every 2 days. Splitting involved dissociation of cells from tissue culture plastic by incubation in Accutase for 5 min and subsequent dilution into PBS. Cells were then centrifuged for 3 min at 1400 rpm, resuspended in new medium and plated onto tissue culture flasks coated with 0.1% gelatin. Cells used in microfluidic experiments were first split into suspension and incubated with 2 µM SYTO 13 (Invitrogen) for 30 min, which stains the nucleus at an intensity 3 to 4 times higher than the cytoplasm, allowing us to detect both nuclear and cytoplasmic signals. The solution was then spun down and resuspended into medium at concentrations of $3x10^6$ cells/ml. For Cytochalasin D treatment, this drug was added 10 min before the experiment at a concentration of 2 µM.[20] For Trichostatin A (TSA) treatment, cells were spun down and resuspended in medium containing 5 µM TSA (Sigma). They were then incubated for 5 hrs, after which SYTO 13 was added and the procedure above was followed.

Image Analysis

We used the following protocol to investigate the cellular and nuclear response to external physical stress. We imaged cells incubated with SYTO 13 before, during and after the constriction. From the fluorescent images we then extracted the cellular and nuclear areas in Matlab using the *MaxEntropy* and *Intermodes* algorithms respectively, which were adapted

This journal is © The Royal Society of Chemistry 20xx

Please do not adjust margins

Please do not adjust margins

from the ImageJ software suite.[21] These were chosen as somewhat conservative thresholding methods that yielded size results similar to those deduced from high resolution microscopy measurements of ES cells and their nuclei in the media condition used in this study.[4] Increasing the sensitivity of thresholding, for example with the *Minimum* thresholding technique, made the thresholding sensitive to small intracellular features such as nucleoli. With major and minor axes of length *a* and *t* before compression respectively, and *a'* and *t'* during compression, the axial strain is given by:

$$S_a = \frac{(a'-a)}{a},$$

while transverse strain is given by:

$$S_t = \frac{(t'-t)}{t}.$$

Statistical Analysis

For the investigation into cell translocation time alteration due to Cytochalasin D treatment, statistical significance was calculated using an n-way ANOVA for the explanatory variables 'cell sample' & 'drug treatment'. Each cell sample was divided equally into a treated and untreated sample. In total 4 samples were used, to produce 4 treated and 4 control samples. ANOVA was also performed to analyze the statistical significance of the strain measurements and standard error of the mean where appropriate.

Results and Discussion

The mechanics of ES cells has been shown to be influenced by their pluripotent state. During differentiation, mechanical changes occur both on a cellular[1,3] and a nuclear level.[4,14] In this paper we present a device that allows rapid mechanical phenotyping of cells and their nuclei. We characterize its capabilities by investigating the response of ES cells to compression in a variety of medium conditions and in response to chemical treatments.

To optimize performance, the microfluidic device was designed with a focus on two major capabilities: compression throughput and run-time before clogging. As ES cells in Serum-LIF medium conditions naturally adhere to substrates, cell aggregates will inevitably form after a certain time.[22] Furthermore, debris, apoptotic cells and aggregates can block the channels as these were designed specifically to apply a small compression to single cells. To alleviate this possibility, the device design first incorporates chip filters around the inlets to filter out objects larger than a single cell (**Figure 1A-C**). Second, the inlet reservoir is split into large channels leading to isolated constriction regions. Hence, if adhering apoptotic cells cause a blockage, this occurs in a single constriction region, so the remaining channels continue to be fully operational.

We optimized the fabrication process and experimental protocol for users who might not be familiar with the technical aspects of microfluidics and might not want to set up high-end dedicated equipment. First, we choose to apply a one-dimensional compression to the ES cells using only the lateral walls but not the top and bottom ones. This allowed for the mold to be produced as a single height layer and to be fabricated in a single step without the use of dedicated photolithography equipment. Also, the one-dimensional approach avoids sharp corners and allows accurate control over the shape of the entrance to the constriction channel, enabling a streamlined approach and passage of cells through the channel without a shift in focal plane intrinsic to the two-dimensional designs. Second, we designed an algorithm to employ different thresholds to isolate the nuclear and cytoplasmic signal. The algorithm has been incorporated into a bespoke Matlab GUI to facilitate rapid semi-automated analysis of all images. As a large number of frames may be recorded during the course of a single experiment, the program first selects only those frames in which cells are detected (**Figure 1E-H**). Then, for these frames the user draws a box around a cell, which is automatically thresholded to highlight the nucleus (or whole cell). This creates a boundary of the nucleus (cell), whose size is measured across the transverse and axial dimensions. Finally, the MATLAB program (**Figure 1I**) calculates the strain of the nucleus (cell) in both dimensions. If more than one cell is present in a frame, the user has the option of drawing a box for each cell to obtain multiple measurements for a single frame. The GUI will be made available, complete with instructions for use, on http://www.stemcells.cam.ac.uk/researchers/principal-investigators/kevin-chalut.

We initially characterized our microfluidic chip by measuring the throughput of cells through the constriction channels as a function of flow rate from 10 to 80 µl/hr. As expected, the relationship was linear at low flow rates, but the number of detected cells was largely constant for values above 40 µl/hr (**Figure 2A**). This is primarily due to the fact that at high flow rates cells translocate the channels very quickly and some of them might not be detected. Therefore, for a flow rate of 40 µl/hr, the upper limit of the linear response of cell throughput, we varied the cell concentration from 1-5 million cells per ml (**Figure 2B**). As expected, the throughput increased linearly with the concentration of cells in the medium. For the experiments below we used a concentration of 3.5 million cells/ml. The maximum flow rate was primarily limited by the frame rate of a typical microscope camera (between 30 and 100 fps). To estimate the accuracy of our size measurements, we flowed fluorescently labelled beads with a mean size of (9.9±0.12) µm through the compression channels. By thresholding the images of the beads (n = 19) outside and inside the compression channels, we measured the diameter of the beads to be (9.98±0.16) µm and (10.07±0.19) µm respectively. This shows that the measurements obtained within this microfluidic device are accurate, and remain consistent while beads pass through the compression channels.

This journal is © The Royal Society of Chemistry 20xx

Please do not adjust margins

Please do not adjust margins

To analyze both strain and recovery of the nuclear and cytoplasmic surface area, we imaged cells before, during and after compression. As expected, the major axis of both the nucleus and cytoplasm increased significantly during compression. However, we did not find evident correlation between axial strain and cell size, and no indication that larger cells (i.e. > 16 µm, the channel height) have a different mechanical response than smaller cells (< 16 µm). Importantly, we also found that cells, even those treated with TSA, a histone deacetylase inhibitor which decondenses chromatin, fully returned to their original values after compression (**Figure 3A & 3B**). The fact that nuclei, even when treated with a chromatin decondensing agent, return to their original sizes, indicates that this technique probes the instantaneous mechanical response of the nucleus without permanently modifying the nuclear structure.

We examined whether the nuclei exhibited a delayed response to the compression as they translocate through the channel, which could be indicative of viscoelastic behavior. To test this, we imaged cells (n = 20) at multiple locations along the length of the channel. Each cell can be observed for multiple frames, or instances, across the channel. For each instance i of cell j we calculated a χ^2-value of the axial strain, defined as

$$\chi^2_{ij,ax} = \frac{(a_{ij,ax} - \bar{a}_{j,ax})^2}{\bar{a}_{j,ax}}$$

where $a_{ij,ax}$ is the axial strain of the nucleus of cell j at the instance i, and $\bar{a}_{j,ax}$ is the average axial strain of all the instances of cell j. Binning the instances according to their position in the first (n=57), middle (n=65) or final (n=69) third of the channel, we found very small χ^2 values with no significant differences between channel positions, indicating that there is no influence of viscoelastic response on our measurements (**Figure 3C**).

Next we treated ES cells with Cytochalasin D, which is an inhibitor of actin polymerization.[20] As cells are more easily deformed due to their lack of polymerized actin filaments, we expected a decrease in translocation time through the constriction channels after treatment with Cytochalasin D. Although there was a high variability between samples, we found that translocation time was indeed significantly shorter for samples treated with Cytochalasin D compared to control samples (**Figure 3D**). These measurements confirmed that this microfluidic device is a high throughput method that can be used for mechanical phenotyping.

To analyze the differential effect of strain on cell nuclei, we set the channel width at 12 µm, larger than the median diameter of the nucleus (11.6±0.2) µm yet smaller than the median cell size (14.3±0.2) µm. Hence, nuclei larger than the approximate diameter of the channel experience compression directly from the sides of the channel. Nuclei smaller than the channel, however, experience this stress to an increasingly smaller extent (decreasing approximately as the inverse of the distance squared due to fluid stress). The cytoplasmic strain resulting from the compression in turn is propagated through the cytoskeleton to the nucleus (**Figure 4A**) as an axial stress. Therefore, we expect the smallest nuclei to primarily experience uniaxial stress along the channel axis, while the largest nuclei would primarily experience uniaxial compression from the channels. Nuclei in the middle of the size distribution would experience a largely biaxial stress.

To distinguish the effects of compression on the cytoplasm and the nucleus while accounting for the size effect, we split the sample for analysis into two subpopulations of cells with large and small nuclei and calculated the strain (**Figure 4B & 4C**). As expected, cells with nuclei larger than the median had a negative transverse cytoplasmic (–0.021±0.008) and nuclear (–0.06±0.01) strain. Both the cytoplasm (0.24±0.02) and the nucleus (0.26±0.03) expanded in the axial direction during compression. However, the axial strain was significantly larger for cells with small nuclei (P < 1e–4) which featured cellular and nuclear axial strain of (0.38±0.04) and (0.46±0.04) respectively. Interestingly, for those cells the transverse nuclear strain was positive yet very close to zero (0.02±0.02), suggesting auxetic nuclei in these conditions, as reported in (Pagliara 2014).[14]

To further explore this observation, we compared the relationship between axial and transverse strain (**Figure 4D**). For small strains, the Poisson's ratio can be approximated by the negative of the transverse over axial strain. Thus, for axial strains smaller than 0.5, we approximated the Poisson's ratio by fitting the nuclear transverse strain versus nuclear axial strain data to a linear function. We aimed to analyse only cells that were experiencing primarily uniaxial stress (either tensile or compressive for small and large nuclei, respectively); therefore, we used only the smallest 25% and largest 25% of nuclei for the analysis. For cells with smaller nuclei, we found a line-fit gradient of 0.30±0.09, compared to 0.15±0.05 for cells with larger nuclei. Given the errors arising from the approximations made, this numbers are in relatively good agreement with one another. The finding indicates a negative Poisson's ratio in the nuclei of these cells, i.e. that these nuclei are exhibiting auxeticity. This can be compared with (Pagliara 2014), in which ES cells at the early stages of differentiation possess auxetic nuclei. In this paper, we are using serum+LIF conditions, which differ from this earlier paper. Serum+LIF conditions should be much more heterogeneous, containing a combination of all three states described in (Pagliara 2014).[14] This method provides a way forward for approximations of Poisson's ratio in cell nuclei.

We tested whether treatment of cells with TSA affected the relationship between compression and strain by modifying the material properties or average size of the nucleus. As chromatin is a primary structural component in the nucleus of ES cells, its decondensation could have a considerable effect on the nuclear response to compression.[23] Hence we examined whether the increase in nuclear deformability due to

 This journal is © The Royal Society of Chemistry 20xx

Please do not adjust margins

Please do not adjust margins

chromatin decondensation (as observed in both Chalut 2012, Krause 2013)[4,23] would increase the magnitude of the axial strain. The proposed device was ideal to investigate this question further. We first observed that TSA treatment had a modest enlarging effect on the median initial nuclear size (11.8±0.2) μm. Second, the nuclear axial strain significantly increased ($P < 0.001$) across the whole population. This could potentially be explained by the larger average nuclear size leading to greater transverse strain. Nonetheless, for cells with nuclei smaller than the median, the mean transverse strain remained stable at 0.006±0.006, while the axial strain increased significantly to 0.68±0.04 ($P < 0.001$). This indicated that small nuclei become more deformable as evidenced by the increase in the axial strain, confirming previous observations but with much higher throughput.

The effect of cell confinement on cellular organization and structure has not yet been extensively studied. As the microfluidic chip presented here, with its single height throughout the chip, allows high-resolution microscopy without a shift in focal plane, we wanted to illustrate the opportunity to apply it to studies of the biological effects of external compression. To demonstrate the potential of the chip, we imaged the actin cortex of a cell line that was stably transfected with a Lifeact-tagRFP plasmid, an actin marker that binds preferentially to F-actin (**Figure 5**). We imaged these cells outside and inside the channels using a spinning disk confocal microscope, and performed a three-dimensional reconstruction of the cellular actin cortex, which showed the presence of the actin cytoskeleton around the edge of the cell at high resolution. In addition, we converted these images to a two-dimensional heatmap of the intensity of the Lifeact signal along the cortex of the whole cell before and during compression, illustrating that the image quality and dimensions are sufficient for further analysis. Hence, the use of this technique, combining high resolution with high throughput microscopy, could be of great utility for future studies investigating structural intracellular changes with compression in single cells.

Conclusions

We have developed a high-throughput microfluidic chip for mechanically phenotyping ES cells. The PDMS chip can easily be produced and used for biological experiments, even by those unfamiliar with microfluidics. We designed a MATLAB GUI to allow swift and easy quantitative analysis of images obtained during experiments. Users can apply thresholding of the images via the GUI, visually assess the automatic detection of the boundary of the nucleus, and obtain size and strain measurements. We showed that the chip is capable of identifying differences in the cellular and nuclear deformability under compression within a sample of ES cells. We found that, in the investigated medium conditions, the nuclei of small cells exhibited a negative Poisson ratio in response to compression. Furthermore, the device was able to detect changes to the mechanical phenotype of cells after treatment with chemical agents such as Cytochalasin D, which decreased the translocation time of the cells through the constrictions. In addition, nuclei of cells treated with TSA were found to have a greater axial strain, indicating greater nuclear deformability, to applied tensile stress than untreated cells. Finally, as a proof-of-principle of the further potential of the device, we showed that it can be used for high-resolution imaging. Thus the chip could in the future be used to investigate, using fluorescent markers, intracellular structural changes in response to compression.

The methodology presented here allows for the identification of mechanical phenotypes of cell compression, with either high throughput or high resolution. These capabilities are particularly relevant when considering the mechanical changes that take place in ES cells as they exit pluripotency and undergo lineage commitment. This feature is not limited to ES cells, however, and this device is well-suited to analyze the mechanical phenotype of other cell types, such as oncogenic cell types, which are heavily influenced by their mechanical environment. In addition, with the aim of promoting or inhibiting growth conditions for culture conditions or cancer treatment, the device can be used to characterize the influence of culture medium on the mechanical responsiveness to stress.

Acknowledgements

This work was supported by the Engineering and Physical Sciences Research Council (A.C.H. and C.M.V.), the Royal Society, UK Medical Research Council and Wellcome Trust (K.J.C), a European Research Council consolidator grant (U.F.K.), Leverhulme Early Career Fellowship (S.P.), the Wellcome Trust and the University of Cambridge (C.L.F.).

Notes and references

1 F. Chowdhury, S. Na, D. Li, Y.-C. Poh, T. S. Tanaka, F. Wang and N. Wang, *Nat Mat*, 2010, **9**, 82-88.
2 M. J. Dalby, N. Gadegaard and R. O. C. Oreffo, *Nat Mater*, 2014, **13**, 558-569.
3 J. D. Pajerowski, K. N. Dahl, F. L. Zhong, P. J. Sammak and D. E. Discher, *PNAS*, 2007, **104(40)**, 15619-15624.
4 K. J. Chalut, M. Höpfler, F. Lautenschläger, L. Boyde, C. J. Chan, A. Ekpenyong, A. Martine-Arias and J. Guck, *Bioph J*, 2012, **103(10)**, 2060-2070.
5 V. Lecault, M. VanInsberghe, S. Sekulovic, D. J. H. F. Knapp, S. Wohrer, W. Bowden, F. Viel, T. McLaughlin, A. Jarandehei, M. Miller, D. Falconnet, A. K. White, D. G. Kent, M. R. Copley, F. Tahipour, C. J. Eaves, R. K. Humphries, J. M. Piret and C. L. Hansen, *Nat Mater*, 2011, **8**, 581-586.
6 G. Velve-Casquillas, M. Le Berre, M. Piel and P. T. Tran, *Nano Today*, 2010, **5(1)**, 28-47.
7 E. K. Sackmann, A. L. Fulton and D. J. Beebe, *Nature*, 2014, **507**, 181-189.
8 W. J. Polacheck, R. Li, S. G. M. Uzel and R. D. Kamm, *Lab Chip*, 2013, **13**, 2252-2267.

Please do not adjust margins

Please do not adjust margins

9 D. R. Gossett, W. M. Weaver, A. J. Mach, S. C. Hur, H. T. Kwong Tse, W. Lee, H. Amini and D. Di Carlo, *Anal Bioanal Chem*, 2010, **397(8)**, 3249-3267.
10 K. Chung, M. M. Crane and H. Lu, *Nature Methods*, 2008, **5**, 637-643.
11 O. Otto, P. Rosendahl, A. Mietke, S. Golfier, C. Herold, D. Klaue, S. Girardo, S. Pagliara, A. Ekpenyong, A. Jacobi, M. Wobus, N. Töpfner, U. F. Keyser, J. Mansfeld, E. Fischer-Friedrich and J. Guck. *Nature Methods*, 2015, **12**, 199-202
12 P. J. Hung, P. J. Lee, P. Sabounchi, R. Lin and L. P. Lee, *Biotechnol Bioeng*, 2005, **89(1)**, 1-8.
13 Y. Zheng, J. Nguyen, Y. Weig and Y. Sun, *Lab Chip*, 2013, **13**, 2464-2483.
14 S. Pagliara, K. Franze, C. R. McClain, G. W. Wylde, C. L. Fisher, R. J. Franklin, A. J. Kable, U. F. Keyser and K. J. Chalut, *Nat Mater*, 2014, **13(6)**, 638-644.
15 M. A. van Zandvoort, C. J. de Grauw, H. C. Gerritsen, J. L. Broers, M. G. oude Egbrink, F. C. Ramaekers and D. W. Slaaf, *Cytometry*, 2002, **47(4)**, 266-235.
16 S. Talwar, N. Jain and G. V. Shivashankar, *Biomaterials*, 2014, **35(8)**, 2411-2419.
17 K. N. Dahl, P. Scaffidi, M. F. Islan, A. G. Yodh, K. L. Wilson and T. Misteli, *PNAS*, 2006, **103(27)**, 10271-10276.
18 M. Zwerger, C. Y. Hoo and J. Lammerding, *Annu Rev Biomed Eng*, 2011, **13**, 397-428.
19 T. Wakayama, I. Rodriguez, A. C. F. Perry, R. Yanagimachi and P. Mombaerts, *PNAS*, 1999, **96(26)**, 14984-14989.
20 J. F. Casella, M. D. Flanagan and S. Lin, *Nature*, 1981, **293**, 302-305.
21 W. S. Rasband, ImageJ, *US National Institute of Health*, http://imagej.nih.gov/ij/, 1997-2015.
22 P. Cartwright, C. McLean, A. Sheppard, D. Rivett, K. Jones and S. Dalton, *Development*, 2005, **132(5)**, 885-96.
23 M. Krause, J. Te Riet and K. Wolf, *Phys Biol*, 2013, **10(6)**, 065002.

 This journal is © The Royal Society of Chemistry 20xx

Please do not adjust margins

Please do not adjust margins

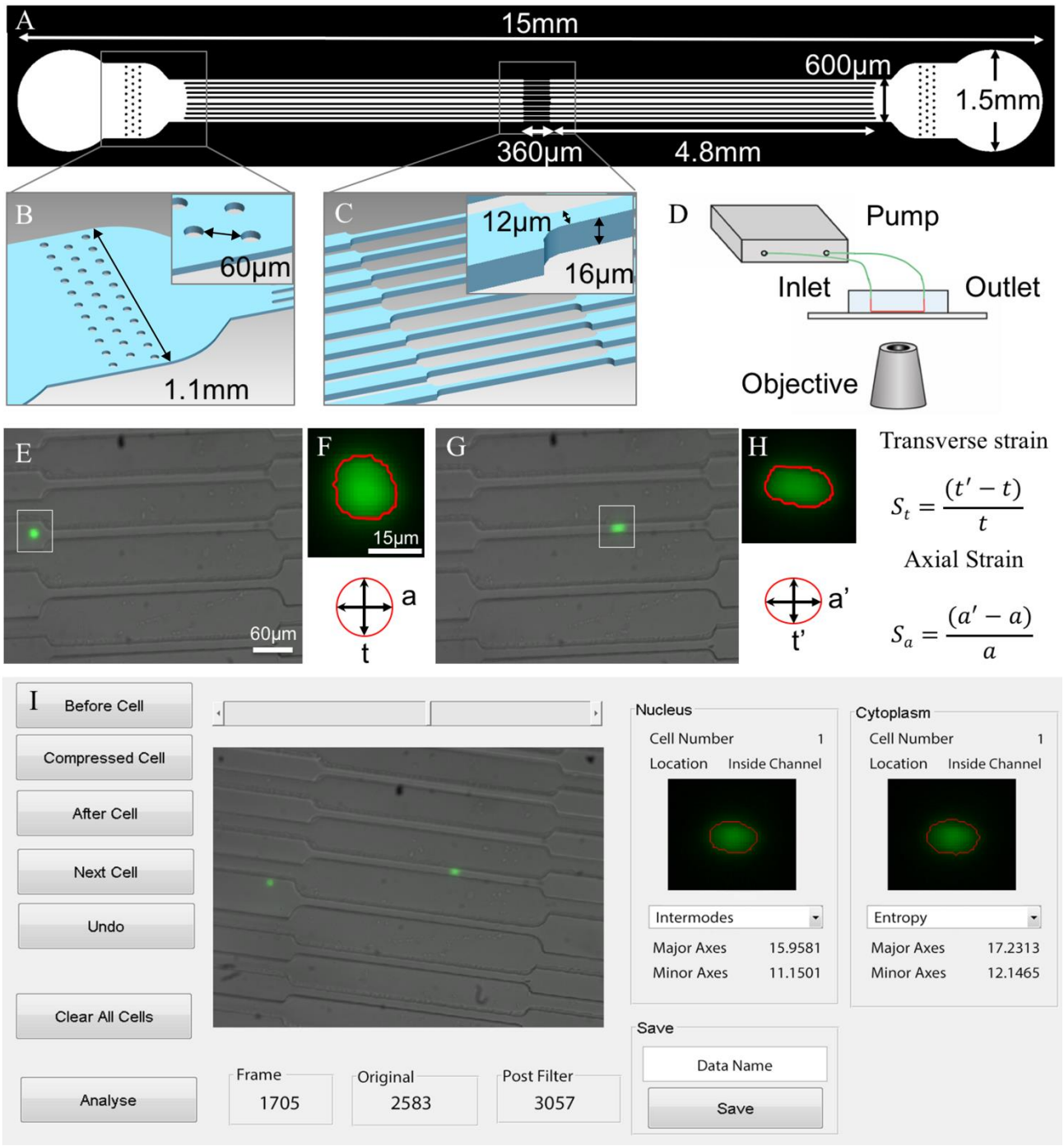

Figure 1: Chip design and experimental setup

(A) Photomask design. The inlet and outlet are situated at the large circular extremes of the design. (B) Expanded view of the inlet. An array of pillars acts as a filter for any object substantially larger than the cells, thus decreasing channel blockages. (C) Cells are guided through separate large channels to the compression channels, where they experience a one-dimensional compression. (D) Experimental set-up: a pressure pump is connected to the chip inlet and outlet via FEP tubing containing cells and media. The pump drives the cells from the inlet to the outlet across the constriction region. (E) Fluorescent image overlaid on bright field image of an ES cell before compression. (F) A region of interest is selected by the user on the GUI for thresholding and measurement. a and t are the axial and transverse dimensions respectively. (G) The ES cell is compressed within a 12 µm constriction channel. (H) A second region of interest is selected to re-threshold the cell under compression. a' and t' are the compressed axial and transverse measurements respectively. The transverse and axial strains are determined using the formulas shown. (I) Screenshot of the MATLAB analysis GUI. The GUI displays the fluorescence image of the cells superimposed on the bright field image of the chip. The user can then see the cells move frame-by-frame towards and through the constriction channels. A box is drawn around the cell of interest by the user, after which the GUI displays the thresholded and measured image in the 'Selected Cell' section of the GUI.

This journal is © The Royal Society of Chemistry 20xx

Please do not adjust margins

Please do not adjust margins

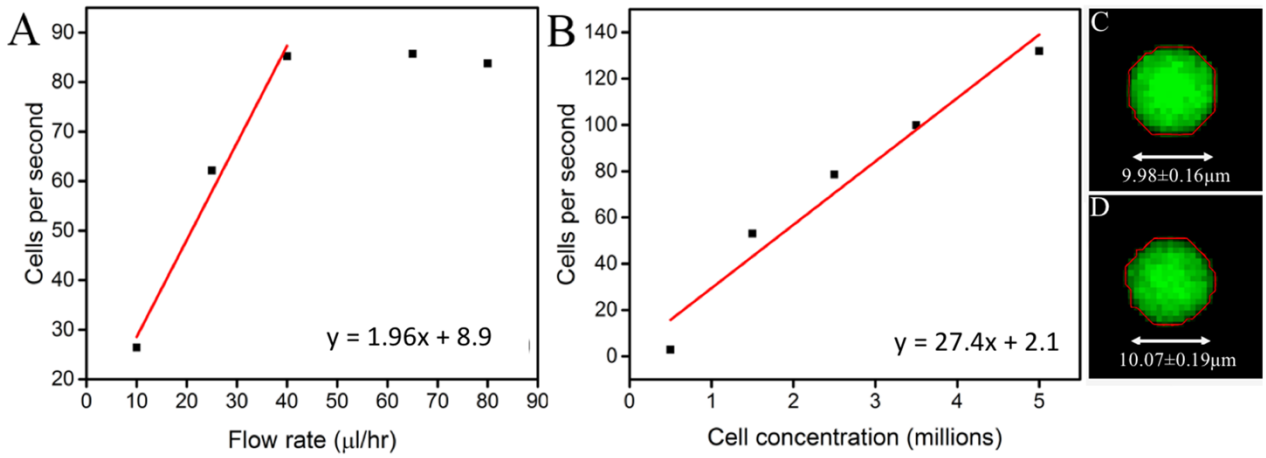

Figure 2: Cell concentration, flow rate and accuracy of size measurements

Cell throughput, measured as number of cells per second, as a function of (A) the flow rate and (B) the initial cell concentration (ROI: 620 x 1100 µm, frame rate: 110 fps). A linear fit has been applied to both plots, however just the first three points of (A) have been utilized. (C & D) Thresholding of (9.9 ± 0.12) µm fluorescently labelled beads (red outline). The mean diameter was measured to be (C) (9.98 ± 0.16) µm outside and (D) (10.07 ± 0.19) µm inside the compression channel (n = 19), illustrating the consistency of our measurement technique.

This journal is © The Royal Society of Chemistry 20xx

Please do not adjust margins

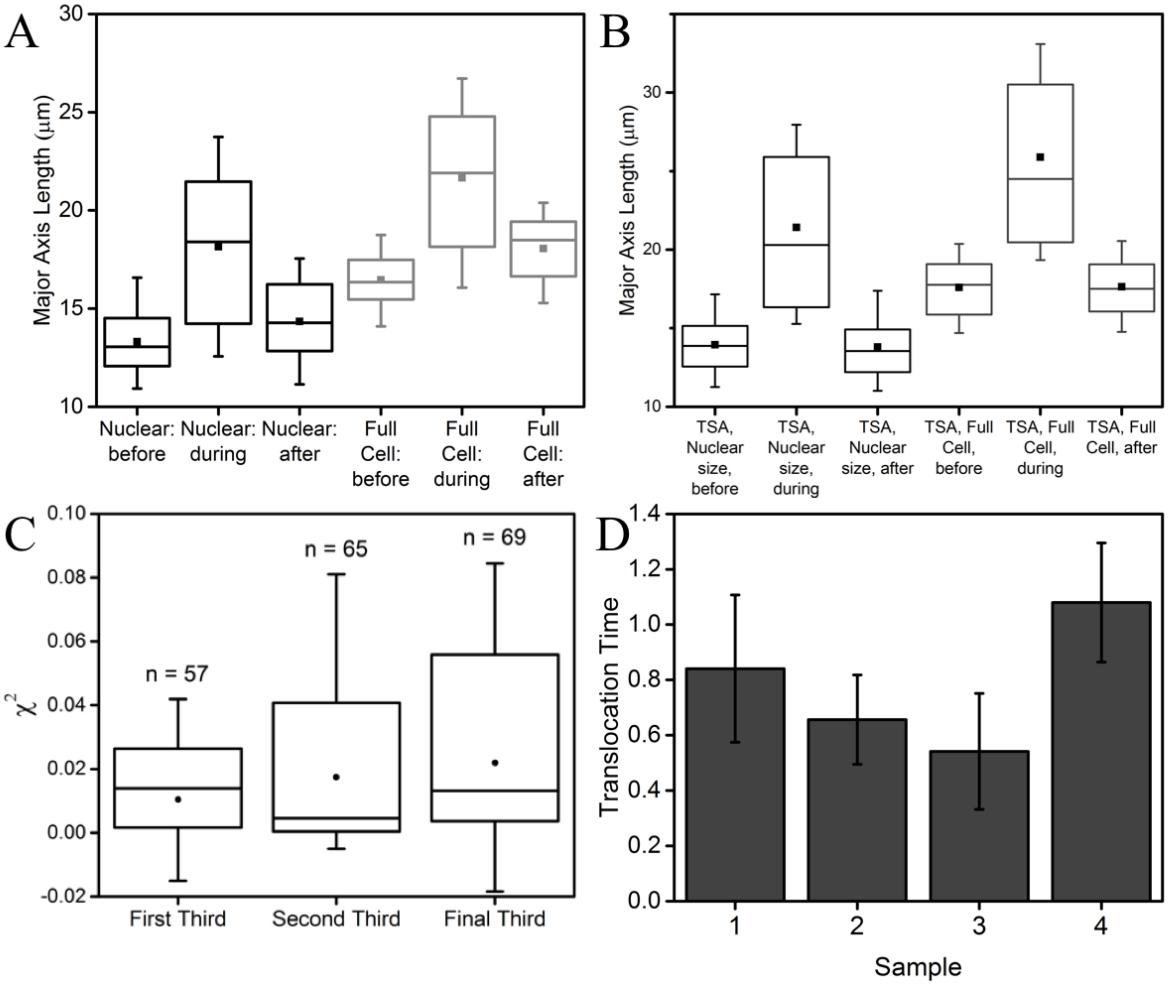

Figure 3: Mechanical phenotyping of ES cells

Length of the nuclear and cellular major axis measured before, during and after compression for (A) control cells (n = 117) and (B) cells treated with Trichostatin A (n = 162). For both the whole cell and the nucleus, the major axial length returned to its approximate original size post-compression. (C) χ^2-value of the cells along the length of the channel. The distributions of χ^2-value of nuclei in the first, middle and final third of the channel are not significantly different. (D) The device was used to characterize cell mechanics by measuring changes in translocation time with cytoskeletal perturbation. Images were captured at 234 fps to record the translocation time, quantified by number of frames elapsed while the cell is in the channel. Cells treated with Cytochalasin D were compared to untreated control cells. Treatment with Cytochalasin D significantly decreased the translocation time ($P << 10^{-4}$, n > 200 cells for each dataset).

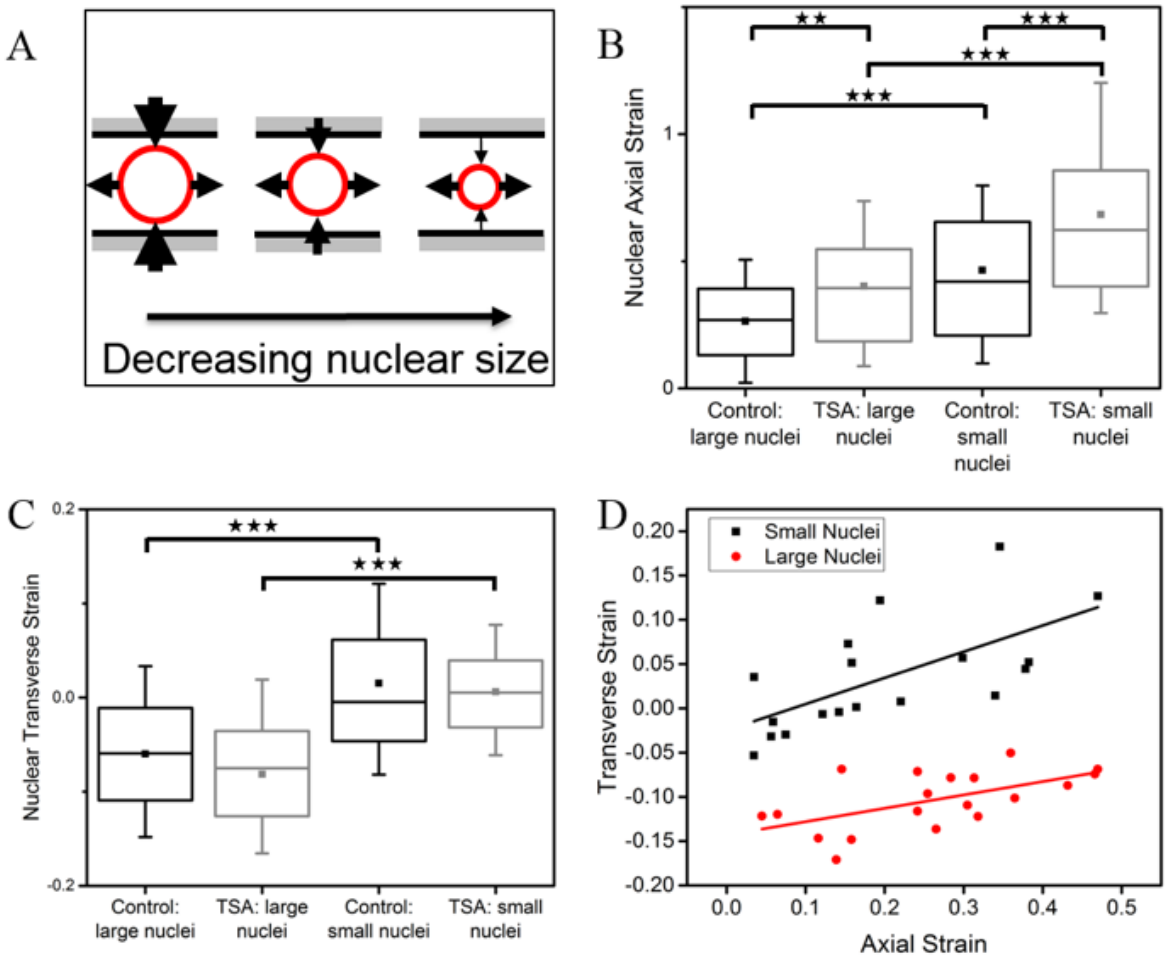

Figure 4: Nuclear mechanics of ES cells

(A) Diagram of forces on the nucleus in response to confinement of cells in the channel. Large cells primarily experience compression forces from the walls of the channel in the transverse direction. As the nuclear size decreases, the compression forces decrease and become more comparable to the tensile forces arising from the elongation of the cell and resulting cytoskeletal stress. With smaller nuclei, the tensile cytoskeletal forces would dominate the compression forces. (B, C) Quantification of nuclear deformability in the (B) axial and (C) transverse direction for control and TSA-treated cells (n = 159 treated, n = 117 control). The nuclei of cells treated with TSA are more deformable, as evidenced by an increase in the magnitude of the axial strains, while the transverse strains are not significantly different. (D) Axial and transverse strain of control ES cell with the smallest nuclei (bottom 25% of size distribution) in black and largest nuclei (largest 25% of the size distribution), with the rationale that these nuclei would be primarily experiencing a uniaxial stress. In the case of uniaxial stress, there is a linear relationship between axial and transverse strain for small strains. Therefore, only axial strains smaller than 0.5 have been plotted. A line of best-fit have been plotted for both small nuclei and large nuclei. Each line has a positive linear relationship between transverse and axial strain (slope of 0.30±0.09 for cells with small nuclei and 0.15±0.05 for cells with large nuclei). The slope in the linear equation is the negative of the Poisson's ration; therefore, both subpopulations exhibit a negative Poisson's ratio.

This journal is © The Royal Society of Chemistry 20xx

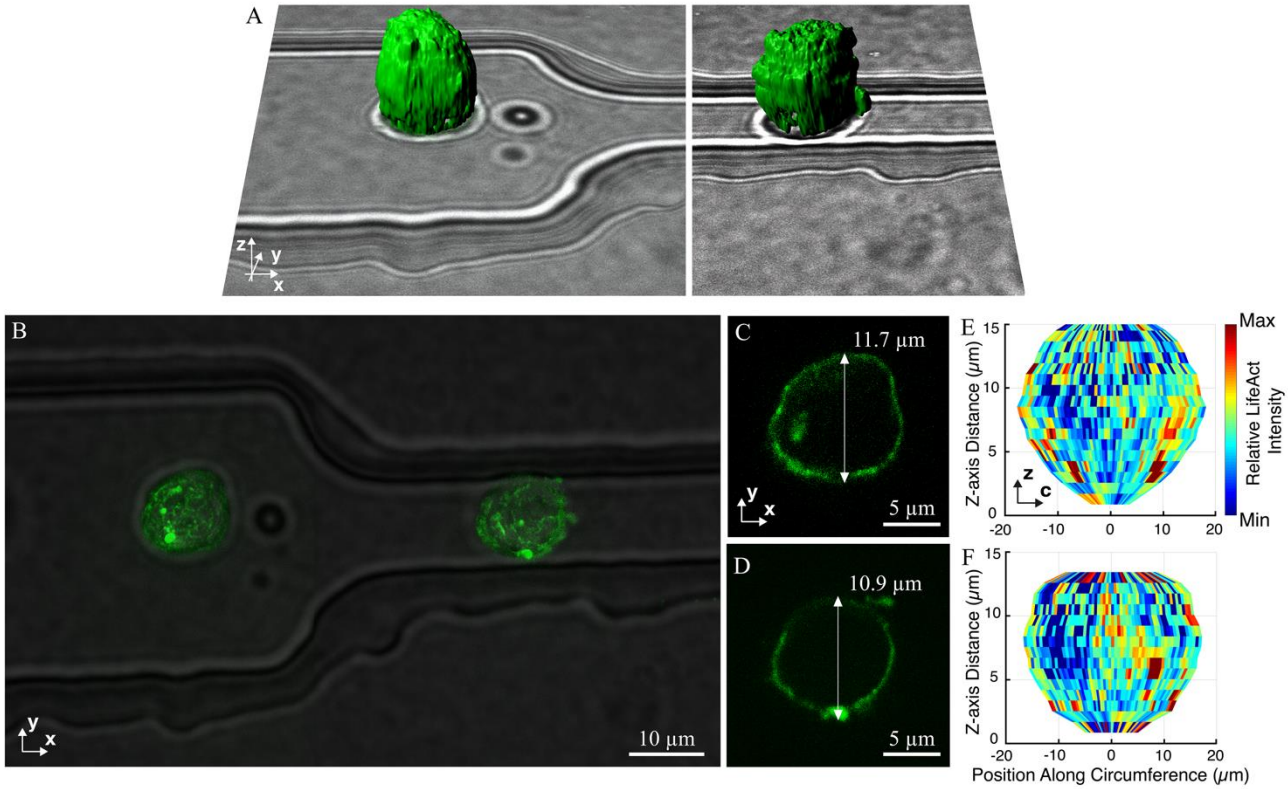

Figure 5: 3D reconstruction of ES cells in confinement

The microfluidic device can be used for confocal microscopy at high numerical aperture of cells containing biological markers to study the intracellular changes that take place in response to confinement. To demonstrate the image quality and level of positional control over the cells within the chip, as well as the possibilities for further analysis, we imaged cells that were transfected with the actin-marker Lifeact within the microfluidic device before and during compression. (A) Composite of two images showing three-dimensional reconstruction of the actin cytoskeleton (green) of a cell before (left) and inside (right) the channel overlaid on the corresponding bright-field images. (B) Maximum projection of the image from the actin network. A slice in the xy-plane through the middle of the cell (C) before and (D) inside the channel. (E, F) Two-dimensional projection of the Lifeact intensity in the cortex of the cell (E) before and (F) inside the channel, with the circumference of the cortex along the horizontal direction.

This journal is © The Royal Society of Chemistry 20xx